Available online at www.sciencedirect.com
SCIENCE DIRECT®
ELSEVIER
International Journal of Solids and Structures 43 (2006) 1009–1022
INTERNATIONAL JOURNAL OF SOLIDS and STRUCTURES
www.elsevier.com/locate/ijsolstr

Measurement of stress intensity factors by digital camera

S.H. Ju *, S.H. Liu, K.W. Liu

Department of Civil Engineering, National Cheng-Kung University, Tainan, Taiwan, ROC

Received 22 October 2004; received in revised form 26 May 2005
Available online 22 July 2005

Abstract

This paper developed a least-squares method to evaluate the mixed-mode stress intensity factors (SIFs) of the isotropic material using the computer images from the digital-camera experiment. This experiment measures the crack opening displacement (COD) and then evaluates SIFs by using the least-squares method. The attractions of this method include: (1) specimen preparation and experiment procedures are not complicated and (2) the isolation of the micro-vibration is not necessary in the experiment. Both finite element simulations and laboratory experiments were applied to validate the current least-squares method with acceptable accuracy, if the even terms of the Irwin's equation are removed.

Keywords: Computer image; Crack; Crack opening displacement; Digital camera; Experiment; Finite element method; Least-squares method; Stress intensity factors

1. Introduction

The main purpose of this paper is to evaluate in-plane stress intensity factors (SIFs), K_I and K_{II}, for a centrally cracked steel plate using the computer images from digital-camera experiments. In the past several years, digital-camera or charge-coupled device (CCD) experiments have been used to fracture mechanics. McNeill et al. (1987) used the computer image correlation of deformed white light speckle patterns in the crack tip to find the SIF. Experimental data for mode-I cracked body problems were presented and compared their study with acceptable analytical results. Nahm et al. (1996) applied the remote measurement system and image processing technique to study the growth behavior of small surface fatigue cracks in 1Cr–1Mo–0.25V steel. The measurement error of the system appeared to be 0.8% and the system could measure down to 30 μm of surface fatigue crack length. Chao et al. (1998) applied the digital image processing to obtain the deformation fields around a propagating crack tip from photographic films recorded

* Corresponding author. Tel.: +886 6 275 7575x63119; fax: +886 6 235 8542.
E-mail address: juju@mail.ncku.edu.tw (S.H. Ju).

0020-7683/$ - see front matter
doi:10.1016/j.ijsolstr.2005.05.052

by a high-speed Cranz–Schardin camera. The in-plane displacements and strains determined from the process were then used to computer the dynamic SIF. Semenski and Jecic (1999) used the reflection method of caustics for application to cracks in mechanically anisotropic materials. To find the exact position of caustics, the experimental images were analyzed by the simple boundary value method and a more sophisticated differential method, which is accomplished by shifting the real image onto the gradient image. Takahashi et al. (2000) presented experimental results which demonstrate restraint of fatigue crack growth in an Al-Mg alloy by wedge effects of fine particles. In their paper, in situ observations of fatigue cracks were performed for the two cases using a CCD microscope, with a magnification of ×1000. The crack length and the crack opening displacement (COD) at the notch root were measured. Machida (2000) measured the point-by-point measurement of in-plane displacement using the pointwise filtering approach of speckle photography. Young's fringes patterns were taken by a CCD and analyzed by the image-processing system. Then, stress-intensity factors were evaluated using the displacement data obtained using speckle photography by applying the least-squares method. Lin (2002) used the digital image and multimedia technology projected in a modified laser shadow spot set-up to engage in a model of the crack growth. With a video CCD camera and frame grabber analyzing, a series of images of laser shadow spot during crack growth was used to evaluate the SIF. Oda et al. (2004) analyzed full field infrared radiometry based on thermoelastic and thermoplastic theory for the non-contact evaluation of stress distributions and deformation in mechanically dissimilar material systems. A CCD camera was employed to investigate the crack tip opening displacement (CTOD) for steel plates loaded in uniaxial tension perpendicular to the weld line.

In the literature, determining mixed-mode SIFs using computer images is limited. This study investigates the accuracy of the least-squares method incorporating the image processing technique to solve mixed-mode fracture problems, and micro-vibration isolation is not necessary during the current experiment.

2. Calculating SIFs using least-squares method

The least-squares method has been applied to the thermoelastic experiments and the finite element method for isotropic and composite materials (Ju, 1996, 1998; Ju et al., 1997; Ju and Rowlands, 2003). In this study, the similar least-squares method incorporating the displacement filed of the isotropic material from the finite element analysis and the digital camera was employed.

2.1. Least-squares method using finite element results

Fig. 1 shows an infinite isotropic plate containing a sharp crack, where x and y are the coordinates of an arbitrary point while the original point of interest is located at the crack tip and the crack surface is in the negative x direction; u and v are the displacement in x and y directions, respectively; r and θ are the polar coordinates. The in-plane displacements, u and v, of a cracked isotropic and linear-elastic plate are (Irwin and Washington, 1957)

$$u=\sum_{n=1}^{\infty}\frac{r^{n/2}}{2\mu}\cdot\left\{a_n^{\mathrm{I}}\left[\left(\kappa+\frac{n}{2}+(-1)^n\right)\cos\frac{n}{2}\theta-\frac{n}{2}\cos\left(\frac{n}{2}-2\right)\theta\right]-a_n^{\mathrm{II}}\left[\left(\kappa+\frac{n}{2}-(-1)^n\right)\sin\frac{n}{2}\theta-\frac{n}{2}\sin\left(\frac{n}{2}-2\right)\theta\right]\right\},\tag{1}$$

$$v=\sum_{n=1}^{\infty}\frac{r^{n/2}}{2\mu}\cdot\left\{a_n^{\mathrm{I}}\left[\left(\kappa-\frac{n}{2}-(-1)^n\right)\sin\frac{n}{2}\theta+\frac{n}{2}\sin\left(\frac{n}{2}-2\right)\theta\right]-a_n^{\mathrm{II}}\left[\left(\kappa+\frac{n}{2}+(-1)^n\right)\cos\frac{n}{2}\theta-\frac{n}{2}\cos\left(\frac{n}{2}-2\right)\theta\right]\right\},\tag{2}$$

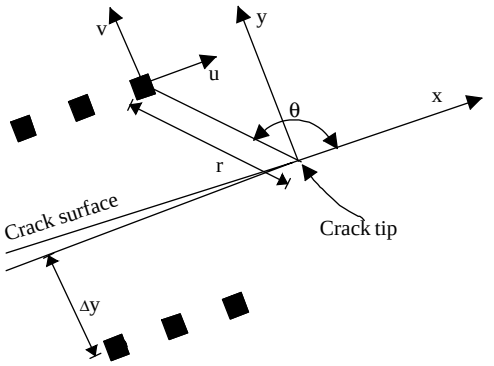

Fig. 1. Infinite plate containing a sharp crack.

where μ is shear modulus, $\kappa = 3 - 4v$ for plane stress and $\kappa = (3 - v)/(1 + v)$ for plane strain, v is Poisson's ratio and a_n^{I} and a_n^{II} are parameters to be determined. Particularly, the first terms of parameters are the function of SIFs as follows:

$$a_1^{\mathrm{I}} = \frac{K_{\mathrm{I}}}{\sqrt{2\pi}} \quad \text{and} \quad a_1^{\mathrm{II}} = \frac{K_{\mathrm{II}}}{\sqrt{2\pi}}. \tag{3}$$

When the first N terms are selected, the matrix forms of Eqs. (1) and (2) are

$$u = [A_1 \;\; A_2 \;\; \cdots \;\; A_N \;\; B_1 \;\; B_2 \;\; \cdots \;\; B_N]\left[a_1^{\mathrm{I}} \;\; a_2^{\mathrm{I}} \;\; \cdots \;\; a_N^{\mathrm{I}} \;\; a_1^{\mathrm{II}} \;\; a_2^{\mathrm{II}} \;\; \cdots \;\; a_N^{\mathrm{II}}\right]^{\mathrm{T}} \text{ or } u = [A]\{a\}, \tag{4}$$

$$v = [C_1 \;\; C_2 \;\; \cdots \;\; C_N \;\; D_1 \;\; D_2 \;\; \cdots \;\; D_N]\left[a_1^{\mathrm{I}} \;\; a_2^{\mathrm{I}} \;\; \cdots \;\; a_N^{\mathrm{I}} \;\; a_1^{\mathrm{II}} \;\; a_2^{\mathrm{II}} \;\; \cdots \;\; a_N^{\mathrm{II}}\right]^{\mathrm{T}} \text{ or } v = [C]\{a\}, \tag{5}$$

where

$$\begin{aligned}
A_n &= \frac{r^{n/2}}{2\mu}\left[\left(\kappa + \frac{n}{2} + (-1)^n\right)\cos\frac{n}{2}\theta - \frac{n}{2}\cos\left(\frac{n}{2} - 2\right)\theta\right],\\
B_n &= \frac{-r^{n/2}}{2\mu}\left[\left(\kappa + \frac{n}{2} - (-1)^n\right)\sin\frac{n}{2}\theta - \frac{n}{2}\sin\left(\frac{n}{2} - 2\right)\theta\right],\\
C_n &= \frac{r^{n/2}}{2\mu}\left[\left(\kappa - \frac{n}{2} - (-1)^n\right)\sin\frac{n}{2}\theta + \frac{n}{2}\sin\left(\frac{n}{2} - 2\right)\theta\right] \quad \text{and}\\
D_n &= \frac{-r^{n/2}}{2\mu}\left[\left(\kappa + \frac{n}{2} + (-1)^n\right)\cos\frac{n}{2}\theta - \frac{n}{2}\cos\left(\frac{n}{2} - 2\right)\theta\right].
\end{aligned} \tag{6}$$

The error for m nodes with u and v displacements from numerical simulations or experimental measurement is

$$\pi = \sum_{i=1}^{m}([A]_i[a] - u_i)^2 + ([C]_i[a] - v_i)^2, \tag{7}$$

where u_i, v_i, $[A]_i$ and $[C]_i$ are the u, v, $[A]$ and $[B]$ of Eqs. (4) and (5) at node i obtained from finite element analyses or the experiments.

To minimize the error by using $\partial\pi/\partial\{a\}$, one obtains

$$[K]\{a\} = \{F\}, \tag{8}$$

where $[K] = \sum_{i=1}^{m}[A]_i^{\mathrm{T}}[A]_i + [C]_i^{\mathrm{T}}[C]_i$ is a symmetric matrix, and $\{F\} = \sum_{i=1}^{m}u_i[A]_i^{\mathrm{T}} + v_i[C]_i^{\mathrm{T}}$.

In this least-squares method, the parameters N, $R_{\max}$ and $R_{\min}$ can be adjusted; N is the number of terms in Eqs. (4) and (5), $R_{\max}$ and $R_{\min}$ are the maximum and minimum radius, respectively, of the area from which data will be included. This study uses $N = 1, \ldots, 8$, $R_{\max}$ = the crack length and $R_{\min} = 0.01$ mm.

2.2. Least-squares method using crack opening displacements from experiments

In the digital-camera experiment of this study, a number of small square symbols on the paper are attached on the specimen with the y-distance, Δy, from the crack surface as shown in Fig. 1. Then, the crack opening displacements (COD) at the symbols in x and y directions are measured. From Eqs. (4) and (5), the COD between symbols in x and y directions, Δu and Δv, can be arranged as follows:

$$\Delta u = [\,U_1 \quad U_2 \quad \cdots \quad U_N\,]\left[\,a_1^{\mathrm{II}} \quad a_2^{\mathrm{II}} \quad \cdots \quad a_N^{\mathrm{II}}\,\right]^{\mathrm{T}} \quad \text{or} \quad \Delta u = [U]\{a^{\mathrm{II}}\}, \tag{9}$$

$$\Delta v = [\,V_1 \quad V_2 \quad \cdots \quad V_N\,]\left[\,a_1^{\mathrm{I}} \quad a_2^{\mathrm{I}} \quad \cdots \quad a_N^{\mathrm{I}}\,\right]^{\mathrm{T}} \quad \text{or} \quad \Delta v = [V]\{a^{\mathrm{I}}\}, \tag{10}$$

where

$$\begin{aligned} U_n &= \frac{-r^{n/2}}{\mu}\left[\left(\kappa + \frac{n}{2} - (-1)^n\right)\sin\frac{n}{2}\theta - \frac{n}{2}\sin\left(\frac{n}{2} - 2\right)\theta\right], \\ V_n &= \frac{r^{n/2}}{\mu}\left[\left(\kappa - \frac{n}{2} - (-1)^n\right)\sin\frac{n}{2}\theta + \frac{n}{2}\sin\left(\frac{n}{2} - 2\right)\theta\right] \end{aligned} \tag{11}$$

and r and θ are located on the non-negative y-coordinate region.

In the experiment, Δy of Fig. 1 is considerably small. If it is zero, θ in Eq. (11) equals π, which causes zero of U_n and V_n for even terms. This condition produces large error of the least-squares method. Alternative is to neglect the even terms of Eqs. (9) and (10) as follows:

$$\Delta u = [\,U_1 \quad U_3 \quad U_5 \quad U_7 \quad \cdots \quad U_N\,]\left[\,a_1^{\mathrm{II}} \quad a_3^{\mathrm{II}} \quad a_5^{\mathrm{II}} \quad a_7^{\mathrm{II}} \quad \cdots \quad a_N^{\mathrm{II}}\,\right]^{\mathrm{T}} \quad \text{or} \quad \Delta u = [U]\{a^{\mathrm{II}}\}, \tag{12}$$

$$\Delta v = [\,V_1 \quad V_3 \quad V_5 \quad V_7 \quad \cdots \quad V_N\,]\left[\,a_1^{\mathrm{I}} \quad a_3^{\mathrm{I}} \quad a_5^{\mathrm{I}} \quad a_7^{\mathrm{I}} \quad \cdots \quad a_N^{\mathrm{I}}\,\right]^{\mathrm{T}} \quad \text{or} \quad \Delta v = [V]\{a^{\mathrm{I}}\}, \tag{13}$$

where N is odd.

Using the same least-squares method for m pairs of displacement symbols, one obtains

$$[K_U]\{a^{\mathrm{II}}\} = \{F_U\} \quad \text{and} \quad [K_V]\{a^{\mathrm{I}}\} = \{F_V\}, \tag{14}$$

where

$$[K_U] = \sum_{i=1}^{m}[U]_i^{\mathrm{T}}[U]_i, \quad [K_V] = \sum_{i=1}^{m}[V]_i^{\mathrm{T}}[V]_i, \quad \{F_U\} = \sum_{i=1}^{m} u_i[U]_i^{\mathrm{T}} \quad \text{and} \quad \{F_V\} = \sum_{i=1}^{m} v_i[V]_i^{\mathrm{T}}. \tag{15}$$

3. Illustration of digital-camera experiment

3.1. Specimens

Three A36 steel specimens (300 mm long, 45 mm wide and 6 mm thick) were used in the digital-camera experiment. The central crack is inclined at 0°, 30° or 50° with respect to the horizontal. The cracks (total length $2a = 30$ mm by 0.3 mm wide) were prepared by electrical discharge machining (EDM). Fig. 2 shows one of the specimens with the crack angle of 30°. Along the crack line, two papers containing two lines of square black symbols were attached on the specimen with Δy of 0.5 mm. The length between two symbol centers is 25/69 mm, and the square symbol size is about 0.2 mm (Figs. 1 and 2). The paper with the thick-

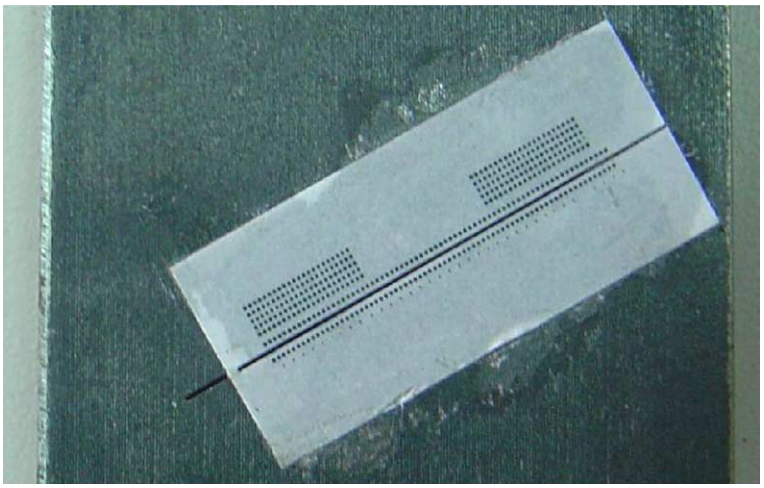

Fig. 2. Details of the A36 steel specimen with the crack angle of 30° (300 mm long, 45 mm wide, 6 mm thick and crack length $a = 15$ mm).

ness of 0.109 mm is commonly used for laser printers. Those square black symbols were printed using a laser printer with the resolution of 600 dpi.

3.2. Digital camera, stereo microscope and illuminant

The Fuji S2 Pro Digital Camera connected to a stereo microscope was used in the experiment as shown in Fig. 3. This camera with 4256×2848-pixel maximum resolution is controlled by a camera shooting software in a personal computer using a direct IEEE1394 cable connection. The shutter speed of 1/125 s and ISO-800 were set in the experiment. The image is saved in the uncompressed TIFF file. The magnification of the stereo microscope is from 7 to 45 times. In the experiment, the working distance between the specimen surface and the microscope edge is about 100 mm with the magnification of 40 times, which can cover the

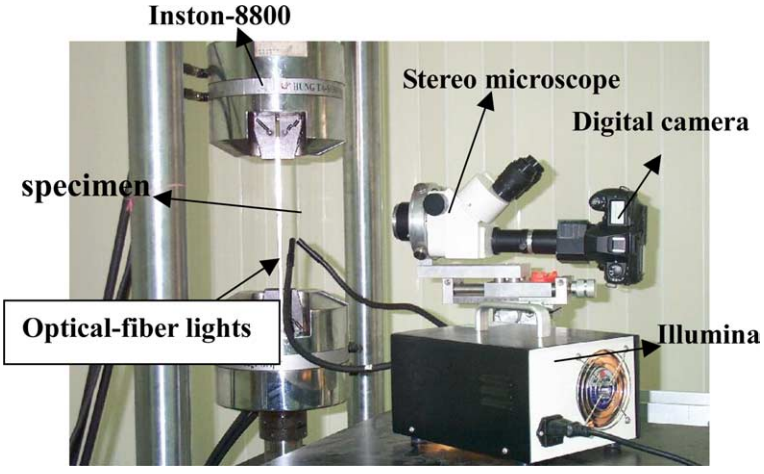

Fig. 3. Details of the experimental system.

image area of 3 mm by 2 mm for the whole resolution of 4256×2848-pixel. The digital camera and stereo microscope are supported on a tripod and allow the adjustment on both horizontal and the vertical directions. The illuminant is two optical-fiber lights transferred from a 20 V–150-W halogens lamp.

3.3. Experimental procedures

The experiment was performed using the Inston-8800 servohydraulic testing machine with a load cell of 100-KN capacity under load control without vibration isolation schemes. The procedures for the experiment are listed below:

(1) Mount the specimen (see Fig. 2) and adjust the microscope–digital-camera system to obtain an image with the area of 3 mm by 2 mm approximately (8 square symbols in the x direction; Fig. 4). At the first time, the image is located near the crack tip.
(2) Set to zero load, and take a picture from the digital camera using the camera shooting software in a personal computer. Then increase load to 10, 15 and 20 kN (stress of 37.04, 55.56 and 74.07 N/mm^2) to take pictures, respectively. All the pictures are stored with the TIFF format.
(3) Adjust the tripod, so the microscope–digital-camera system is allowed to move to the next section for observation (gradually move to the crack center), and then repeat procedure (2). After the image near the crack center is taken, stop the test.

3.4. Evaluation of displacements from computer images

After the experiment, a Fortran program CCD3 (http//myweb.ncku.edu.tw/~juju/index.htm) can be used to calculate the x and y centers of the square symbols of each picture. The displacements at the centers of those square symbols are obtained from their coordinate difference between the W-load and zero-load pictures, where W is the load of 10, 15 or 20 kN used in this paper. Thus, CODs in x and y directions are calculated from the displacement difference between upper and bottom square symbols. The procedures of the program CCD3 are illustrated as follows:

(1) Read the TIFF file and obtain the red, green and blue (RGB) values at each pixel (totally, 4256×2848 pixels). Subroutine RIMAGE (about 120 statements) in CCD3 program performs this procedure.
(2) This step finds the region of each square symbol. Since the RGB values of the pixels in a square symbol are much different from those of other place. The CCD3 program finds the regions that have the similar RGB value of the square block. The programming algorithm is similar to the polygon filling of the computer graphics. Subroutine GP (about 100 statements) in CCD3 program performs this procedure. Since the symbol, area and size are known, too large or too small regions that are noises or wrong regions will be skipped.
(3) Calculate the x and y centers of each region of the square symbol for this current picture. It must be noted that the size of the square symbol is too small (about 0.2 mm), so it is often not a good square shape. This situation will not cause trouble, since the CCD3 program can find the region that has the certain RGB values, and the square shape is not necessary.
(4) Go to step 1 for the next picture. Until finishing the last picture, stop the program.

Fig. 4a and b shows the images (TIFF files) taken from the digital camera for the specimen with the crack angle of 30° under the loads of 0 and 20 kN. Fig. 4c shows the positions of square symbols using the CCD3 program. Blue symbols are the positions under a zero load and red symbols are the positions under a 20-kN tensile load. The displacement of each symbol can be clearly seen in Fig. 4c.

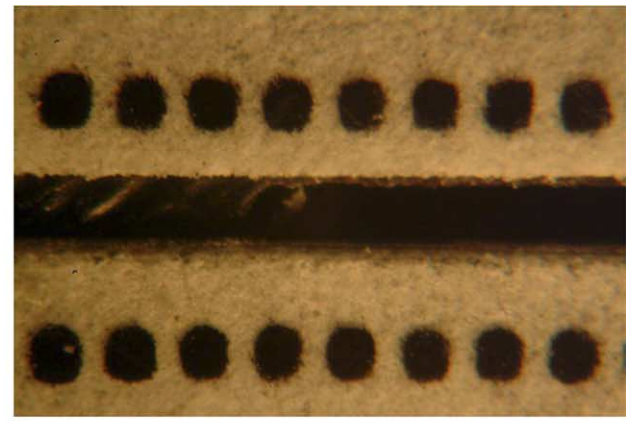

(a)

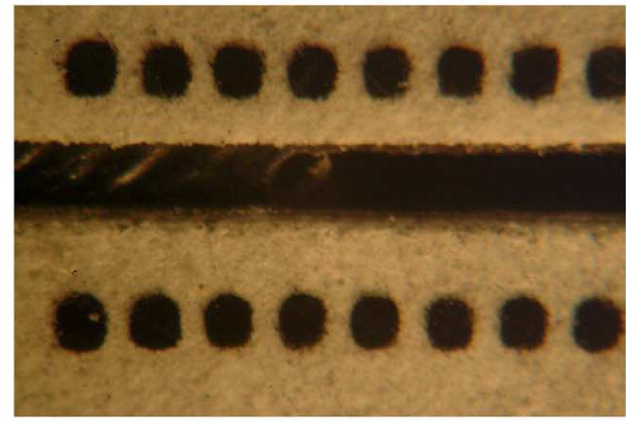

(b)

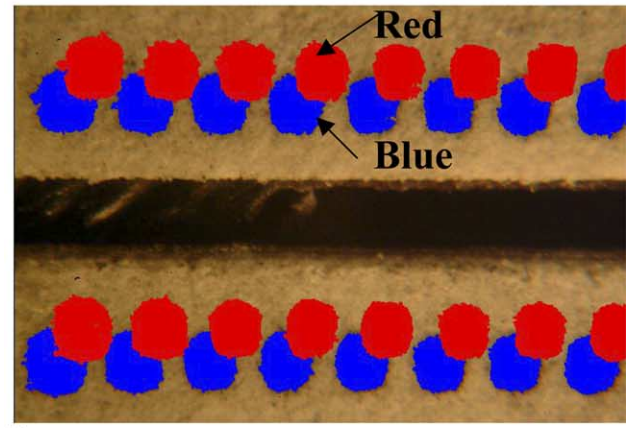

(c)

Fig. 4. Computer images taken from the digital camera and generated from the CCD3 program for the specimen with the crack angle of 30° under loads of 0 and 20 kN. (a) Image from the digital camera (TIFF file) without load. (b) Image from the digital camera (TIFF file) under the load of 20 kN. (c) Image from the CCD3 program under loads of 0 and 20 kN.

4. Numerical validation

Numerical analysis were conducted initially using the finite element analysis. These finite element predictions provide the input for Eq. (8) as well as the simulated experimental input COD values for Eq. (14). Eight-node quadrilateral isoparametric elements were utilized in the finite element meshes; furthermore, quarter-point singular isoparametric elements (Henshell and Shaw, 1975) were employed around the crack tip. All numerical analysis assume linear-elastic, plane-stress conditions. The applied stress, S, in each case is unity and the material is steel (Young's modulus $E = 204$ GPa and Poisson's ratio $v = 0.29$).

The problem is a center slant cracked rectangular plate subjected to uniform unixial tensile stress as shown in Fig. 5a. The SIFs of this problem were solved by Kitagawa and Yuuki (1977) using the modified mapping collocation method. The crack angle (α) is set to 15°, 30° or 60°, and the crack length over the

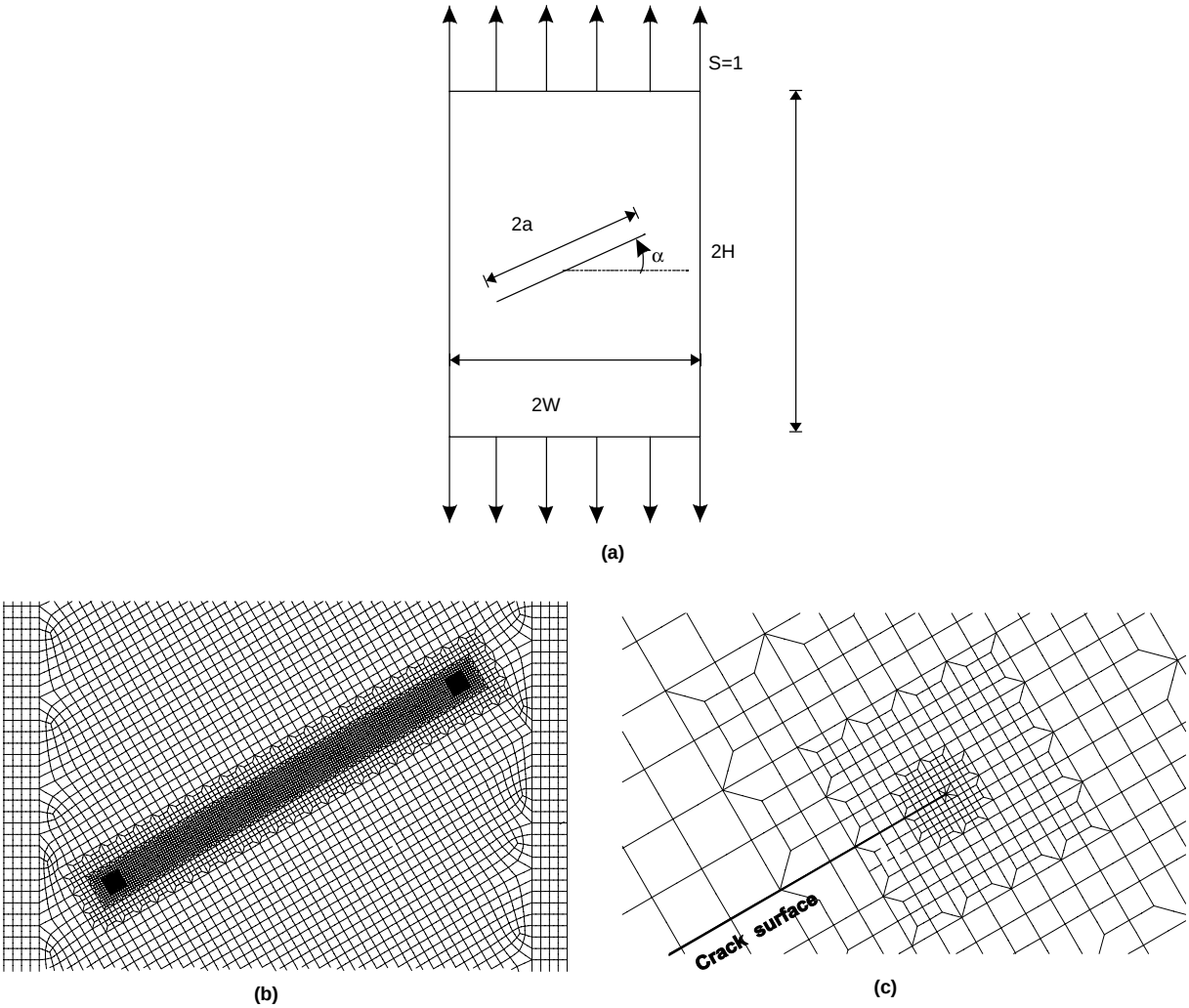

Fig. 5. Model and finite element mesh of a center slant cracked rectangular plate subjected to uniform unixial tensile stress for numerical validation. (a) Model illustration for the problems of numerical validation ($H = 2W$). (b) Finite element mesh of near the crack of $\alpha = 30°$ and $a/W = 0.7$. (c) Finite element mesh very near the upper right crack tip.

specimen width (a/W) is set to 0.4, 0.6 or 0.7. The finite element mesh near the crack of $\alpha = 30°$ and $a/W = 0.7$ is shown in Fig. 5b and c. The error of the least-squares method and the equivalent SIFs are defined as follows:

$$\text{Error} = \frac{|K^{\text{Ref}} - K^{\text{LS}}|}{|K^{\text{Ref}}|}, \tag{16}$$

$$F_{\text{I}} = K_{\text{I}}^{\text{LS}}/\left(S\sqrt{\pi a}\right) \quad \text{and} \quad F_{\text{II}} = K_{\text{II}}^{\text{LS}}/\left(S\sqrt{\pi a}\right), \tag{17}$$

where K^{Ref} is the stress intensity factor K_{I} or K_{II} obtained from Kitagawa and Yuuki (1977), K^{LS} is that calculated from the least-squares method, S is the applied stress at far field and a is the crack length.

4.1. Accuracy of the least-squares method using finite element results

The variations of SIFs affected by N (from 1 to 9) were investigated as shown in Table 1 using Eq. (8), where the SIFs of Table 1 are averaged under $R_{\max} = 2$, 5 and 10 mm and $R_{\min} = 0.01$ mm. Table 1 indicates that the least-squares results agree well with the referenced SIFs except $N \leqq 2$. This means that the

Table 1
Least-squares results and errors of numerical experiments

N	F_{I}	F_{II}	N	F_{I}	F_{II}	N	F_{I}	F_{II}
$\alpha = 15°$ and $a/W = 0.4$			$\alpha = 15°$ and $a/W = 0.6$			$\alpha = 15°$ and $a/W = 0.7$		
1	1.0126 (0.027)	0.2118 (0.173)	1	1.1878 (0.025)	0.2069 (0.241)	1	1.3457 (0.023)	0.1939 (0.331)
2	1.0024 (0.036)	0.2537 (0.009)	2	1.1747 (0.036)	0.2697 (0.010)	2	1.3301 (0.035)	0.2883 (0.006)
3	1.0371 (0.003)	0.2556 (0.001)	3	1.2113 (0.006)	0.2723 (0.001)	3	1.3635 (0.011)	0.2917 (−0.006)
4	1.0384 (0.002)	0.2555 (0.002)	4	1.2145 (0.003)	0.2718 (0.003)	4	1.3691 (0.006)	0.2907 (−0.002)
5	1.0393 (0.001)	0.2555 (0.002)	5	1.2166 (0.001)	0.2721 (0.001)	5	1.3748 (0.002)	0.2915 (−0.005)
6	1.0393 (0.001)	0.2555 (0.002)	6	1.2168 (0.001)	0.2723 (0.001)	6	1.3754 (0.002)	0.2924 (−0.008)
7	1.0393 (0.001)	0.2555 (0.002)	7	1.2169 (0.001)	0.2721 (0.001)	7	1.3765 (0.001)	0.2926 (−0.009)
8	1.0393 (0.001)	0.2554 (0.002)	8	1.2170 (0.001)	0.2722 (0.001)	8	1.3769 (0.001)	0.2928 (−0.010)
9	1.0393 (0.001)	0.2555 (0.002)	9	1.2170 (0.001)	0.2722 (0.001)	9	1.3767 (0.001)	0.2928 (−0.010)
$\alpha = 30°$ and $a/W = 0.4$			$\alpha = 30°$ and $a/W = 0.6$			$\alpha = 30°$ and $a/W = 0.7$		
1	0.8166 (0.034)	0.3442 (0.235)	1	0.9562 (0.028)	0.3428 (0.286)	1	1.0678 (0.021)	0.3415 (0.328)
2	0.8122 (0.040)	0.4399 (0.022)	2	0.9505 (0.034)	0.4664 (0.028)	2	1.0611 (0.027)	0.4900 (0.035)
3	0.8439 (0.002)	0.4488 (0.002)	3	0.9807 (0.003)	0.4777 (0.005)	3	1.0862 (0.004)	0.5039 (0.008)
4	0.8445 (0.001)	0.4490 (0.002)	4	0.9808 (0.003)	0.4781 (0.004)	4	1.0855 (0.005)	0.5045 (0.007)
5	0.8451 (0.001)	0.4488 (0.002)	5	0.9823 (0.002)	0.4783 (0.004)	5	1.0886 (0.002)	0.5050 (0.006)
6	0.8452 (0.001)	0.4489 (0.002)	6	0.9825 (0.002)	0.4786 (0.003)	6	1.0891 (0.002)	0.5061 (0.004)
7	0.8451 (0.001)	0.4489 (0.002)	7	0.9826 (0.001)	0.4786 (0.003)	7	1.0895 (0.001)	0.5063 (0.003)
8	0.8451 (0.001)	0.4489 (0.002)	8	0.9827 (0.001)	0.4786 (0.003)	8	1.0898 (0.001)	0.5065 (0.003)
9	0.8451 (0.001)	0.4489 (0.002)	9	0.9827 (0.001)	0.4786 (0.003)	9	1.0898 (0.001)	0.5065 (0.003)
$\alpha = 60°$ and $a/W = 0.4$			$\alpha = 60°$ and $a/W = 0.6$			$\alpha = 60°$ and $a/W = 0.7$		
1	0.2771 (0.043)	0.3670 (0.212)	1	0.3246 (0.026)	0.3844 (0.234)	1	0.3549 (0.012)	0.3893 (0.257)
2	0.2810 (0.030)	0.4626 (0.007)	2	0.3283 (0.015)	0.4967 (0.011)	2	0.3585 (0.001)	0.5165 (0.014)
3	0.2896 (0.000)	0.4655 (0.001)	3	0.3344 (−0.004)	0.4997 (0.005)	3	0.3616 (−0.007)	0.5197 (0.008)
4	0.2895 (0.000)	0.4654 (0.001)	4	0.3331 (0.000)	0.5001 (0.004)	4	0.3593 (−0.001)	0.5205 (0.007)
5	0.2899 (−0.001)	0.4653 (0.002)	5	0.3340 (−0.002)	0.4999 (0.005)	5	0.3605 (−0.004)	0.5203 (0.007)
6	0.2899 (−0.001)	0.4654 (0.001)	6	0.3340 (−0.003)	0.5001 (0.004)	6	0.3606 (−0.004)	0.5207 (0.006)
7	0.2899 (−0.001)	0.4653 (0.001)	7	0.3340 (−0.002)	0.5001 (0.004)	7	0.3605 (−0.004)	0.5208 (0.006)
8	0.2899 (−0.001)	0.4653 (0.001)	8	0.3340 (−0.002)	0.5001 (0.004)	8	0.3605 (−0.004)	0.5208 (0.006)
9	0.2899 (−0.001)	0.4653 (0.001)	9	0.3340 (−0.002)	0.5001 (0.004)	9	0.3605 (−0.004)	0.5208 (0.006)

The value inside () means the error calculated from Eq. (16).

least-square method incorporating the finite element result can evaluate the SIFs accurately for $N \geqq 3$. Moreover, the accuracy is also independent of R_{max}. For practice, R_{max} should be smaller than the crack length to avoid including other singular data and R_{min} can equal a very small value to only exclude the singularity at the crack tip.

4.2. Accuracy of the least-squares method using simulated COD values

The least-squares method of equations in Section 2.2 is used with the simulated COD from finite element results. Since experimental input values usually contain some scatter error, those simulated COD data from finite element analyses were subsequently modified according to the following equation:

$$S = S_{original}(1 + RAN * P_{factor}), \tag{18}$$

where values of S computed by Eq. (18) now become the input for the least-squares method, such that $S_{original}$ is the 'perfect' x- or y-COD obtained from the finite element analysis; RAN is a random value between -1 and 1, and P_{factor} is a user-selected factor. In this study P_{factor} is set to 0, 0.1 and 0.4, in which 0.4 means that the maximum error over $S_{original}$ can extend to 40%.

The variations of SIFs affected by P_{factor} (0, 0.1 and 0.4), N (from 1 to 9) and Δy (0, 0.25 and 0.5 mm; Fig. 1) were investigated under the combinations of three crack angles of 15°, 30° or 60° and three a/W of 0.4, 0.6 or 0.7, so there are total 9 cases for a certain P_{factor}, N and Δy. First, Eqs. (9), (10), and (14) are used, which means that the even terms are not removed. At this condition, Eq. (14) is singular for $\Delta y = 0$ and no solution can be obtained. For $\Delta y = 0.25$ and 0.5 mm, Table 2 shows the averaged errors of least-squares results, where the averaged error is the mean error value (Eq. (16)) of the 9 cases (the combinations of three crack angles and three a/W). Table 2 shows the following features:

Table 2
Averaged errors of least-squares results using Eqs. 9, 10, 14

N	K_I-error	K_{II}-error	N	K_I-error	K_{II}-error	N	K_I-error	K_{II}-error
$P_{factor} = 0$ and $\Delta y = 0.25$ mm			$P_{factor} = 0.1$ and $\Delta y = 0.25$ mm			$P_{factor} = 0.4$ and $\Delta y = 0.25$ mm		
1	0.162	0.233	1	0.171	0.242	1	0.199	0.267
2	0.277	0.364	2	0.273	0.360	2	0.261	0.349
3	0.050	0.035	3	0.073	0.041	3	0.139	0.088
4	0.087	0.078	4	0.078	0.058	4	0.093	0.113
5	0.012	0.074	5	0.081	0.210	5	0.331	0.620
6	0.013	0.104	6	0.309	0.283	6	0.715	0.738
7	0.040	0.125	7	0.143	0.369	7	2.287	2.356
8	0.065	0.047	8	0.626	2.869	8	2.380	13.052
9	0.137	0.198	9	7.625	47.163	9	32.857	90.139
$P_{factor} = 0$ and $\Delta y = 0.5$ mm			$P_{factor} = 0.1$ and $\Delta y = 0.5$ mm			$P_{factor} = 0.4$ and $\Delta y = 0.5$ mm		
1	0.161	0.246	1	0.171	0.254	1	0.198	0.279
2	0.287	0.382	2	0.281	0.377	2	0.265	0.361
3	0.053	0.037	3	0.073	0.045	3	0.132	0.091
4	0.097	0.109	4	0.099	0.117	4	0.103	0.149
5	0.017	0.119	5	0.184	0.727	5	0.754	2.549
6	0.031	0.070	6	0.293	0.733	6	1.119	1.592
7	0.127	0.084	7	0.817	0.423	7	7.658	0.952
8	0.143	0.081	8	0.419	0.700	8	5.399	2.119
9	0.090	0.222	9	3.693	0.401	9	17.433	1.601

Averaged error is the mean value of Eq. (16) for the 9 cases from the combinations of three crack angles and three a/W.

(1) For $P_{\text{factor}} = 0$ and $N = 1$ or 2, the errors are large and generally the calculated SIFs cannot be used. For $N > 2$, the errors are still much larger than those of Table 1, which means that the least-squares results are not stable when Eqs. (9) and (10) are applied.
(2) When a small scatter error is given ($P_{\text{factor}} = 0.1$), the errors of least-squares results increasing proportional to N are considerably large except for $N = 3$. For a larger scatter error ($P_{\text{factor}} = 0.4$), the condition is even worse.
(3) Generally, the errors are larger for smaller Δy. The reason is because a smaller Δy produces more singular result of Eq. (14).

Then, Eqs. (12)–(14) are used, which means that the even terms are removed. At this condition, Eq. (14) will not be singular for $\Delta y = 0$. Table 3 shows the averaged errors of least-squares results, which indicate the following features:

(1) For $P_{\text{factor}} = 0$ and $N = 1$, the error is large and generally the calculated SIFs cannot be used. For $N \geqq 3$, the errors are small and similar to those of Table 1, which means that the least-squares results are stable when even terms are removed.
(2) Although the least-squares errors increase slowly proportional to P_{factor}, they are not sensitive to the scatter errors. This means that the least-squares method using Eqs. (12) and (13) can average the scatter errors of the input data. When scatter errors are large but averaged values of them are small, which means that the measured data are located positively and negatively along the correct data, the errors of this least-squares method can be small too.
(3) Generally, the error is larger for a larger Δy. The reason is because the least-squares method using Eqs. (12) and (13) that remove the zero terms is only correct for $\Delta y = 0$. When Δy increases, the approximation intensity of the least-squares method using Eqs. (12) and (13) will also increase. Thus, when Δy is not large, the accuracy of this least-squares method can be acceptable.

Table 3
Averaged errors of least-squares results using Eqs. (12)–(14)

N	K_{I}-error	K_{II}-error	N	K_{I}-error	K_{II}-error	N	K_{I}-error	K_{II}-error
$P_{\text{factor}} = 0$ and $\Delta y = 0$ mm			$P_{\text{factor}} = 0.1$ and $\Delta y = 0$ mm			$P_{\text{factor}} = 0.4$ and $\Delta y = 0$ mm		
1	3.119	2.832	1	3.083	2.798	1	2.973	2.696
3	0.027	0.019	3	0.020	0.018	3	0.016	0.033
5	0.002	0.008	5	0.020	0.009	5	0.076	0.062
7	0.001	0.003	7	0.020	0.021	7	0.081	0.080
9	0.003	0.006	9	0.019	0.020	9	0.079	0.077
$P_{\text{factor}} = 0$ and $\Delta y = 0.25$ mm			$P_{\text{factor}} = .1$ and $\Delta y = 0.25$ mm			$P_{\text{factor}} = .4$ and $\Delta y = 0.25$ mm		
1	0.162	0.233	1	0.171	0.242	1	0.199	0.267
3	0.028	0.031	3	0.013	0.048	3	0.048	0.099
5	0.005	0.048	5	0.009	0.054	5	0.033	0.072
7	0.006	0.054	7	0.008	0.050	7	0.021	0.037
9	0.006	0.063	9	0.013	0.058	9	0.043	0.041
$P_{\text{factor}} = 0$ and $\Delta y = 0.5$ mm			$P_{\text{factor}} = 0.1$ and $\Delta y = 0.5$mm			$P_{\text{factor}} = 0.4$ and $\Delta y = 0.5$ mm		
1	0.161	0.246	1	0.171	0.254	1	0.198	0.279
3	0.028	0.056	3	0.012	0.073	3	0.047	0.123
5	0.010	0.084	5	0.014	0.084	5	0.024	0.085
7	0.012	0.099	7	0.015	0.093	7	0.040	0.075
9	0.014	0.111	9	0.019	0.108	9	0.035	0.100

Averaged error is the mean value of Eq. (16) for the 9 cases from the combinations of three crack angles and three a/W.

5. Experimental results

In this section, the least-squares method is applied to evaluate the SIFs of the experiments illustrated in Section 3. Fig. 6 shows parts of the CODs measured by the digital camera and calculated by the finite element method. This figure indicates that the two results are in good agreement. For the digital-camera experiment, the least-squares results are the averaged values under $N = 3$, 5 and 7 using Eqs. (12)–(14) (even terms are removed). The referenced SIFs for comparison as shown in Table 4 are calculated using the least-squares method of Eq. (8) with the condition of $R_{max} = 5$ mm, $R_{min} = 0.01$ mm and $N = 8$. Table 5 shows the experimental results evaluated by the least-squares method. This table indicates that the SIF error of the digital-camera experiment is about 8%, which should be acceptable for the mixed-mode fracture problem. From out further investigation, most of the errors or scatters of experiment results are due to the distortion of the microscope. This condition can sometimes produce about 2-pixel difference between a

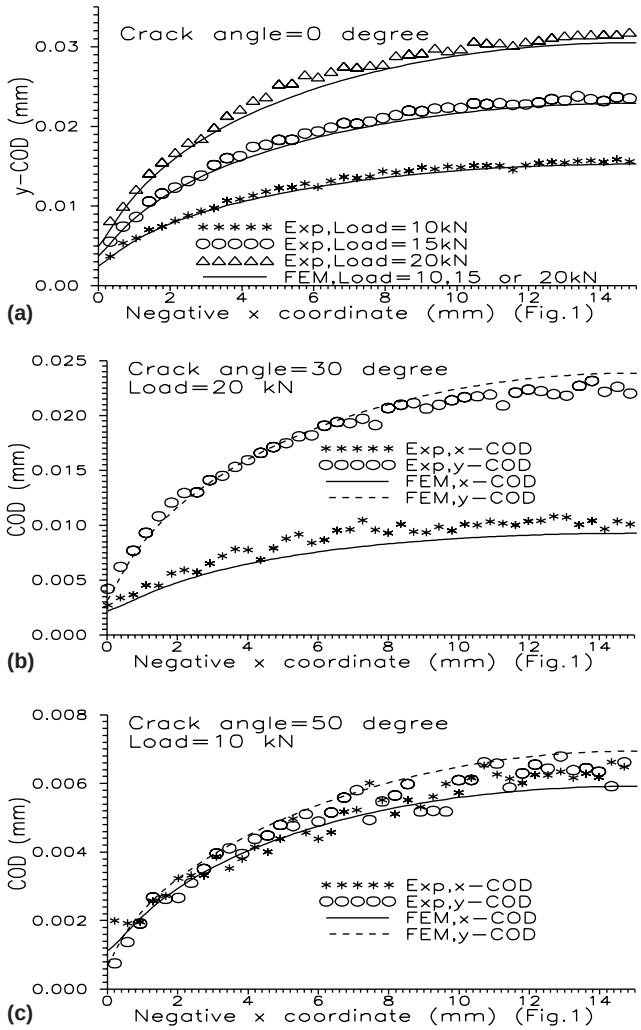

Fig. 6. Comparison of CODs between experimental and finite element results. (a) y-COD under load of 10, 15 or 20 kN for crack angle of 0°. (b) x- and y-COD under load of 20 kN for crack angle of 30°. (c) x- and y-COD under load of 10 kN for crack angle of 50°.

Table 4
Least-squares SIFs using finite element analyses for specimens in Fig. 2

$\alpha = 0°$		$\alpha = 30°$		$\alpha = 50°$	
F_I	F_{II}	F_I	F_{II}	F_I	F_{II}
1.416	0.000	1.050	0.4958	0.5786	0.5765

Table 5
Least-squares SIFs using experimental results for specimens in Fig. 2

Applied stress (N/mm^2)	$\alpha = 0°$		$\alpha = 30°$		$\alpha = 50°$	
	F_I	F_{II}	F_I	F_{II}	F_I	F_{II}
74.07	1.5361 (−0.085)	0.0904 (–)	1.1400 (−0.086)	0.4967 (−0.002)	0.5620 (0.025)	0.6193 (−0.074)
55.56	1.5123 (−0.068)	0.0795 (–)	1.1384 (−0.084)	0.4581 (0.076)	0.5522 (0.042)	0.5536 (0.040)
37.04	1.5016 (−0.060)	0.0721 (–)	1.1230 (−0.069)	0.4203 (0.152)	0.5483 (0.049)	0.5280 (0.084)

The value inside () means the error calculated from Eq. (16), where K^{Ref} is obtain from Table 4.

certain location. The micro-vibration and illumination of the experimental system are not dominated. Thus, to improve the experimental accuracy, it is suggested that a precise microscope or a distortion calibration procedure be used.

6. Conclusion

This paper developed a least-squares method to find the mixed-mode SIFs of the isotropic material using the digital-camera experiment, in which two papers containing two lines of square black symbols were attached on the specimen along the crack. Then, a digital camera connected to a stereo microscope was used to measure the displacement of each symbol so that the CODs of the crack can be evaluated. Finally, the least-squares method was applied to calculate SIFs using the measured CODs. Finite element simulations and laboratory experiments were performed to validate that the accuracy of the current least-squares method is acceptable if the even terms of the Irwin's equation (Irwin and Washington, 1957) are removed. The advantages of this method include: (1) specimen preparation and experiment procedures are not complicated and (2) the isolation of the micro-vibration is not necessary, if the shutter speed is appropriately arranged, and normally 1/60 to 1/125 s can be set when a servohydraulic testing machine is used.

Acknowledgement

This study was supported by the National Science Council, Republic of China, under contract number: NSC90-2218-E-006-063.

References

Chao, Y.J., Luo, P.F., Kalthoff, J.F., 1998. An experimental study of the deformation fields around a propagating crack tip. Experimental Mechanics 38, 79–85.

Henshell, R.D., Shaw, K.G., 1975. Crack tip elements are unnecessary. International Journal for Numerical Method in Engineering 9, 495–509.

Irwin, G.R., Washington, D.C., 1957. Analysis of stresses and strains near the end of a crack traveling a plate. Transaction of ASME, Journal of Applied Mechanics 24, 361–364.

Ju, S.H., 1996. Simulating stress intensity factors for anisotropic materials by the least squares method. International Journal of Fracture 81, 283–297.

Ju, S.H., 1998. Simulating three-dimensional stress intensity factors by the least-squares method. International Journal for Numerical Method in Engineering 43, 1437–1451.

Ju, S.H., Rowlands, R.E., 2003. Thermoelastic Determination of K_I and K_{II} in an orthotropic graphite/epoxy composite. Journal of Composite Materials 37, 2011–2025.

Ju, S.H., Lesniak, J.R., Sandor, B.I., 1997. Finite element simulation of stress intensity factors via the thermoelastic technique. Experimental Mechanics SEM 37, 278–284.

Kitagawa, H., Yuuki, R., 1977. Analysis of arbitrarily shaped crack in a finite plate using conformal mapping, 1st report-construction of analysis procedure and its applicability. Transactions of the Japanese Society for Mechanical Engineering 43, 4354–4362.

Lin, C.S., 2002. Pilot-type scientific experimental device using optical method and computer vision technology. INDILAN Journal of Pure and Applied Physics 40 (NOV), 816–827.

Machida, K., 2000. Study of stress-analyzing system by speckle photography. JSME International Journal Series A—Solid Mechanics and Material Engineering 43, 343–350.

McNeill, S.R., Peters, W.H., Sutton, M.A., 1987. Estimation of stress intensity factor by digital image correlation. Engineering Fracture Mechanics 28, 101–112.

Nahm, S.H., Lee, H.M., Suh, C.M., 1996. A study on observation and growth behavior of small surface cracks by remote measurement system. KSME Journal 10, 396–404.

Oda, I., Willett, A., Yamamoto, M., Matsumoto, T., Sosogi, Y., 2004. Non-contact evaluation of stresses and deformation behaviour in pre-cracked dissimilar welded plates. Engineering Fracture Mechanics 71, 1453–1475.

Semenski, D., Jecic, S., 1999. Experimental caustics analysis in fracture mechanics of anisotropic materials. Experimental Mechanics 39, 177–183.

Takahashi, I., Takahashi, C., Kotani, N., 2000. Restraint of fatigue crack growth by wedge effects of fine particles. Fatigue and Fracture of Engineering: Materials and Structures 23, 867–877.